Nanoscale

PAPER

View Article Online
View Journal | View Issue

Cite this: *Nanoscale*, 2018, **10**, 22319

Reliability of rare-earth-doped infrared luminescent nanothermometers†

Lucía Labrador-Páez, [a,b] Marco Pedroni, [a,c] Adolfo Speghini, [c] José García-Solé, [a,b] Patricia Haro-González [a,b] and Daniel Jaque *[a,b]

Received 17th September 2018,
Accepted 26th October 2018

DOI: 10.1039/c8nr07566b

rsc.li/nanoscale

The use of infrared-emitting rare-earth-doped luminescent nanoparticles as nanothermometers has attracted great attention during the last few years. The scientific community has identified rare-earth-doped luminescent nanoparticles as one of the most sensitive and versatile systems for contactless local temperature sensing in a great variety of fields, but especially in nanomedicine. Researchers are nowadays focused on the design and development of multifunctional nanothermometers with new spectral operation ranges, outstanding brightness, and enhanced sensitivities. However, no attention has been paid to the assessment of the actual reliability of the measurements provided by rare-earth-doped luminescent nanothermometers. In fact, it is assumed that they are ideal temperature sensors. Nevertheless, this is far from being true. In this work we demonstrate that the emission spectra of rare-earth-doped nanothermometers can be affected by numerous environmental and experimental factors. These include the numerical aperture of the optical elements used for their optical excitation and luminescence collection, the local concentration of nanothermometers, optical length variations, self-absorption of the luminescence by the nanothermometers themselves, and solvent optical absorption. This work concludes that rare-earth-doped luminescent nanothermometers are not as reliable as thought and, consequently, special care has to be taken when extracting temperature estimations from the variation of their emission spectra.

Introduction

Luminescence nanothermometry, *i.e.* the use of luminescent nanoparticles as contactless local thermometers, has experienced a remarkable development during the last few years.[1–3] The possibility offered by luminescent nanothermometers (LNThs) for remote thermal sensing has been highly appealing for researchers working in diverse areas, ranging from electronics to materials characterization.[4–7] However, it is in the area of nanomedicine where LNThs have found the most innovative applications. For instance, LNThs have made it possible to fully control thermal therapies and to develop new methods for diagnosis.[8–11] In particular, rare-earth-doped LNThs (RE-LNThs) have already demonstrated their leading role as probes in nanomedicine. RE-LNThs have been used, for instance, to measure intracellular temperature and to achieve *in vivo* intratumoral temperature control during photothermal treatments.[9,12] Their good performance relies on the possibility of tailoring their absorption and emission bands by conveniently choosing the rare-earth dopants, so that they would both lie within the near-infrared biological windows (allowing subcutaneous thermal sensing), the low dosage needed (even a single nanoparticle), low cytotoxicity, easy surface functionalization, and high thermal sensitivity.[1,13–15] During the last few years, the tailoring of their structure by core–shell engineering has allowed the improvement of not only their brightness and thermal sensitivity, but also their multifunctionalization. RE-LNThs with the core–shell structure can now also be used for activating chemical therapies or drug delivery and multiplexing sensing processes, and even for achieving treat-and-see therapies.[3,9,15–17]

Nevertheless, certain factors have remained overlooked in the design and use of RE-LNThs. The emission of the luminescent ions is susceptible to alteration by some experimental or external factors, whose effects have been traditionally underestimated by the scientific community. Our previous experience with the use of RE-LNThs has revealed some sources of artefacts during the sensing process, which may finally result in a false reading from the sensor. In general, artefacts may arise from system inhomogeneities,[18] from the limitations of the experimental procedure or detection system,[19] from the interference of contaminants or external signals,[20] but also from an

[a]*Fluorescence Imaging Group, Departamento de Física de Materiales, Universidad Autónoma de Madrid, 28049, Spain. E-mail: daniel.jaque@uam.es*
[b]*Instituto universitario de ciencia de materiales Nicolás Cabrera, Universidad Autónoma de Madrid, 28049, Spain*
[c]*Nanomaterials Research Group, Dipartimento di Biotecnologie, Università di Verona and INSTM, UDR Verona, I-37134, Italy*

†Electronic supplementary information (ESI) available. See DOI: 10.1039/c8nr07566b

unexpected dependence of the system's response under the experimental conditions.[21,22] The latter is the case under scrutiny in this work. For instance, the dependence of the rare-earth ion emission (band shape and/or branching ratios) on the applied excitation power is a well-known process. As a consequence, special precautions are taken when using RE-LNThs to retain the applied excitation power constant. Nevertheless, significant differences could arise between the applied and the on-target excitation power densities, especially in nanomedicine due to the complicated propagation of light through tissues and fluids. Note that a great variety of processes can lead to significant alterations in the on-target excitation power density: the absorption of the emitted luminescence by the environment, the deformation of the focal volume due to changes of the refractive index and optical aberrations, *etc*. These modifications may lead to an erroneous measured value due to the fact that a fixed applied excitation power density may result in a quite different on-target excitation power density. The other possible factor altering the spectral shape of RE-LNThs is the partial self-absorption (SA) of their luminescence. This process takes place when the excitation and emission spectra overlap each other. This requirement is fulfilled for rare-earth ions in the case of optical transitions involving the fundamental energy level. If SA takes place, the longer the path of the luminescence through the sample volume, the more probable its partial reabsorption, and so the more altered the resulting emission spectrum. Consequently, the magnitude of this artefact depends on the experimental conditions. The SA of the luminescence was extensively studied years ago for rare-earth-doped bulk luminescent materials, especially for those with applications as lasing hosts or in telecommunication devices.[23–29] Recently this effect has been observed for the first time at the nanoscale when comparing the spectrum of a single Er^{3+}-doped luminescent nanoparticle ($^4F_{9/2} \rightarrow {}^4I_{15/2}$ transition) with that of a set of them by means of optical trapping of a controlled number of luminescent nanoparticles.[30] However, the magnitude and relevance of SA in colloidal solutions of rare-earth-doped luminescent nanoparticles have not been explored yet, as they are considered as diluted systems. However, this is far from being true, as SA can be observed in colloidal dispersions of luminescent nanoparticles and so it could be a source of error in the reading provided by RE-LNThs. Temperature measurements can also be altered by the optical absorption of the luminescence by the environment. If the absorption of the environment (solvent, biological fluid, or tissue) shows a certain overlap with the emission of the employed RE-LNThs, then the resulting luminescence could show changes not related to temperature variations, but, instead, to this artefact.

Despite the diverse experimental factors leading to false temperature readings, these have not been investigated in the past, to the best of our knowledge. For the sake of raising awareness about the importance of this matter, we will examine the reliability of RE-LNThs by evaluating how their luminescence is influenced by the abovementioned artefacts. Table 1 includes some representative studies on luminescence

Table 1 RE-LNThs employing Tm^{3+} and Nd^{3+}, the solvent/environment where they were immersed (tissue: chicken breast, DMEM: cell culturing medium), the observed emission bands, the procedure for temperature reading from the emission spectra, the calibration temperature range, and their susceptibility to the artefacts studied in this work

Material	Solvent/ environment	Emission bands	Measurement procedure	Temp. range	Exc. power dens.	Self-abs.	Solvent abs.	Ref.
$NaYF_4$:Yb,Tm@CaF_2	Powder	$^3H_4 \rightarrow {}^3H_6$ and $^1G_4 \rightarrow {}^3H_6$	Ratio (Stark)	40–100 °C	Yes	Yes (both)	No	31
$NaYF_4$:Yb,Tm@$NaYF_4$:Pr	Cyclohexane	$^1G_4 \rightarrow {}^3F_4$ and $^3F_{2,3} \rightarrow {}^3H_6$	Ratio	29–237 °C	Yes	Yes ($^3F_{2,3} \rightarrow {}^3H_6$)	No	32
$NaNbO_3$:Yb,Tm	Water	$^1G_4 \rightarrow {}^3H_6$	Ratio (Stark)	24–140 °C	No	Yes	No	35
CaF_2:Tm,Yb	PBS	$^3H_4 \rightarrow {}^3H_6$	Ratio (Stark)	26–48 °C	No	Yes	No	34
$NaNbO_3$:Tm	Powder, water, tissue	$^1G_4 \rightarrow {}^3H_5$ and $^3H_4 \rightarrow {}^3H_6$	Ratio (Stark)	30–98 °C	Yes	Yes	No	33
$LiLaNdYbP_4O_{12}$	Powder	Yb^{3+}:$^2F_{5/2} \rightarrow {}^2F_{7/2}$ and Nd^{3+}: $^4F_{3/2} \rightarrow {}^4I_{13/2}$	Ratio	−180–390 °C	Yes	Yes (Yb), no (Nd)	Yes	36
$(GdNd)_2O_3$	Powder	$^4F_{3/2} \rightarrow {}^4I_{13/2}$	Ratio (Stark)	30–130 °C	No	No	Yes	37
$(Gd_{1-x}Nd_x)_2O_3$	Powder	$^4F_{3/2} \rightarrow {}^4I_{9/2}$ and $^4F_{5/2} \rightarrow {}^4I_{9/2}$	Ratio	15–50 °C	Yes	Yes	No	46
$NaYF_4$:Nd	Powder	$^4F_{3/2} \rightarrow {}^4I_{9/2}$	Ratio (Stark)	0–150 °C	No	Yes	No	45
LaF_3:Nd	Water	$^4F_{3/2} \rightarrow {}^4I_{9/2}$	Ratio (Stark)	20–60 °C	No	Yes	No	41
LaF_3:Nd	Water	$^4F_{3/2} \rightarrow {}^4I_{9/2}$	Ratio (Stark)	20–60 °C	No	Yes	No	42
YVO_4:Nd	Water	$^4F_{3/2} \rightarrow {}^4I_{11/2}$	Ratio peak–valley	26–58 °C	No	No	No	38
$NaGdF_4$:Yb,Ho,Er@$NaGdF_4$: Yb@$NaGdF_4$:Yb,Nd	Hexane, water, D_2O, DMEM, tissue	Nd^{3+}:$^4F_{3/2} \rightarrow {}^4I_{13/2}$,$Er^{3+}$: $^4I_{13/2} \rightarrow {}^4I_{15/2}$ and Ho^{3+}: $^5I_6 \rightarrow {}^5I_8$	Ratio	20–50 °C	Yes	Yes	Yes	47
LaF_3:Nd	Powder, phantom tissue	$^4F_{3/2} \rightarrow {}^4I_{9/2}$	Ratio (Stark)	10–60 °C	No	Yes	No	39
LaF_3:Nd	Water, tissue	$^4F_{3/2} \rightarrow {}^4I_{9/2}$	Ratio (Stark)	25–65 °C	No	Yes	No	40
LaF_3:Nd	Powder, water, tissues (chicken breast, mouse skin and muscle)	$^4F_{3/2} \rightarrow {}^4I_{9/2}$	Ratio (Stark)	33–73 °C	No	Yes	No	43
$Y_3Al_5O_{12}$:Nd	Powder, water, tissue	$^4F_{3/2} \rightarrow {}^4I_{9/2}$	Ratio (Stark)	15–70 °C	No	Yes	No	44
LaF_3:Nd@LaF_3:Yb	Water, *in vivo* (mouse)	Yb^{3+}:$^2F_{5/2} \rightarrow {}^2F_{7/2}$ and Nd^{3+}:$^4F_{3/2} \rightarrow {}^4I_{13/2}$	Ratio	10–50 °C	Yes	Yes (Yb), no (Nd)	Yes	15

nanothermometry employing Tm^{3+} and Nd^{3+}-doped LNThs.[15,31–47] These are the most common rare-earth doping ions for nanothermometry in bioapplications, as they emit within the biological windows of transparency of tissues. The temperature was obtained in these cases by the ratiometric analysis of their emission spectra. This is the most frequently employed method in RE-LNTh-based luminescence nanothermometry, as it is supposed to provide a temperature measurement that is, in principle, independent of the variations of their luminescence intensity.[1,3] However, it is the shape of the emission spectra and not their intensity that the abovementioned artefacts would affect, leading us to a false result.

In this work, we have identified as possible sources of artefacts (i) the excitation power dependence of emission spectra, (ii) the SA of the luminescence by the RE-LNThs themselves, and (iii) the partial absorption of the RE-LNTh luminescence by the surrounding media. Assessing the magnitude of the error in the temperature reading due to these artefacts is the main objective of this work. Moreover, the dependence of these artefacts on some experimental parameters is studied to provide strategies for the enhancement of the accuracy and reliability of RE-LNThs. Finally, an overview of the emission bands of trivalent rare-earth ions within the biological windows of transparency of tissues that are susceptible to these artefacts is included.

Results and discussion

As shown in Table 1, most of the recent studies in the field of infrared emitting RE-LNThs deal with Nd^{3+}, Yb^{3+}, and Tm^{3+} as doping ions. These ions are specially suitable for luminescence thermometry in biological systems due to the possibility of optical excitation in the first biological window (700–950 nm) and their emission bands spanning the first and second biological windows (1000–1350 nm).[47,48] Most studies in Table 1 use fluoride matrixes, which have reduced quenching due to their low phonon energy. Thus, as representative examples of RE-LNThs for biological applications, the RE-LNThs studied in this work are SrF_2:0.218Yb,0.002Tm nanocrystals dispersed in D_2O and SrF_2:0.5Nd nanocrystals dispersed in H_2O. SrF_2 nanoparticles doped with lanthanide ions have been used previously for nanothermometry,[49,50] bioimaging,[51] fundamental spectroscopy studies,[30] and optical trapping,[52] among other applications. The sizes were 9.5 ± 1.4 nm and 9.6 ± 1.5 nm, respectively, according to the transmission electron microscopy images (see Fig. 1). Their hydrodynamic size obtained by dynamic light scattering measurements is close to the size determined by TEM, as shown in ESI Fig. S1.† Fig. 1 also shows optical images of the colloidal dispersions of RE-LNThs, which show excellent stability, remaining dispersed for months. These RE-LNThs were selected due to their temperature-sensitive emission spectra, as shown in Fig. 1. The sensitivity of a LNTh can be assessed by the thermal relative sensitivity (S_R), which is defined as:

$$S_R = \frac{1}{R}\frac{dR}{dT} \quad (1)$$

where R is the intensity ratio from the spectra and T is the temperature. The temperature-induced spectral changes in SrF_2:0.218Yb,0.002Tm LNTh emission provide a ratiometric thermal relative sensitivity (S_R) of 0.24% $°C^{-1}$ (numerical aperture (NA) 0.6, concentration 5 mg mL^{-1} in D_2O, 8×10^7 mW cm^{-2} applied excitation power density, minimum depth). In the case of SrF_2:0.5Nd LNThs, the temperature-induced spectral changes of

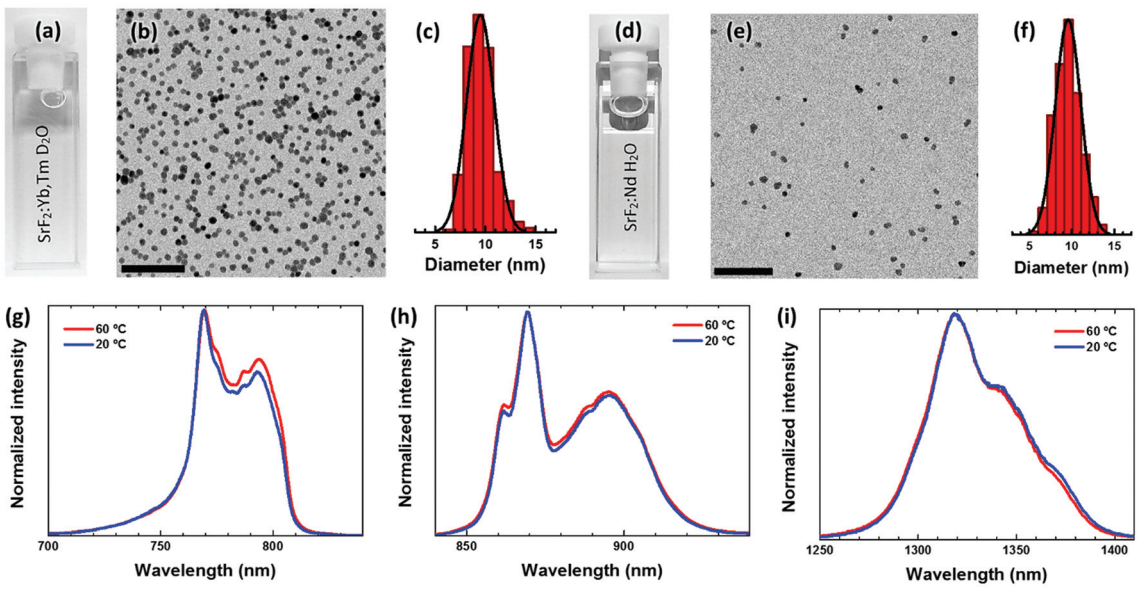

Fig. 1 RE-LNThs employed in this work. (a), (d) Optical images of colloidal dispersions, (b), (e) transmission electron microscopy images (scale bars: 100 nm), (c), (f) size distributions obtained from diverse transmission electron microscopy images, and emission spectra at different temperatures for (g) SrF_2:Yb,Tm nanoparticles in D_2O and (h), (i) SrF_2:0.5Nd nanoparticles in H_2O in different spectral ranges, respectively.

the emission bands at 880 and 1320 nm lead to S_R of 0.17 and 0.25% °C^{-1}, respectively (NA 0.6, concentration 5 mg mL^{-1} in H_2O, 8 × 10^7 mW cm^{-2} applied excitation power density, minimum depth). These S_R values are not a breakthrough in the state-of-the-art, but they are comparable to the S_R previously reported for other RE-LNThs, which have demonstrated to be high enough to perform measurements in biological systems. In the following we describe the experimental evidence of how uncontrolled variations of experimental conditions could lead to unexpected errors in the temperature reading from RE-LNThs. In particular, we evidence how uncertainties could arise due to the uncontrolled modification of on-target power densities, the self-absorption of the luminescence by RE-LNThs and the intrinsic absorption of the solvent.

Temperature uncertainties due to uncontrolled changes of the on-target power density

The SrF_2:Yb,Tm emission band at around 780 nm, frequently employed in the past for subcutaneous temperature sensing, consists of two overlapping emission bands of Tm^{3+} ions.[31–35] One of them peaks at 769 nm ($^1G_4 \rightarrow {}^3H_5$ transition), while the other one peaks at 795 nm ($^3H_4 \rightarrow {}^3H_6$ transition, see Fig. 2a). This energy level diagram shows that the emission at 769 nm is generated after a three photon excitation process, whereas the emission at 795 nm is originated by a two-photon excitation process. Thus, their emission intensities show a different dependence on the applied excitation power density, which goes with the n power of the applied excitation power, where n is the number of photons involved in the process. Fig. 2b shows the emission spectra of SrF_2:Yb,Tm LNThs at different excitation power densities. At minimum excitation power, the emission coming from the $^3H_4 \rightarrow {}^3H_6$ transition (795 nm, two photon excitation) dominates. However, at the highest excitation power the $^1G_4 \rightarrow {}^3H_5$ transition (769 nm, three photons) is the most intense one, as its intensity increases at a faster rate with the applied excitation power (see Fig. S2†). Fig. 2c shows the intensity ratio between these emission peaks for different excitation powers, which shows a change up to 49% mW^{-1} at low excitation power. Thus, a reduction in the excitation power and a temperature increase have a similar effect on the emission spectra of this RE-LNTh. This drawback could be easily overcome by performing all the measurements using a constant excitation power density. Nevertheless, even in the case when the applied excitation power is kept constant, the actual excitation power density reaching the RE-LNThs could become altered by experimental parameters typically disregarded in luminescence nanothermometry experiments. For instance, different focus depths in a liquid medium could lead to relevant changes in the local excitation power density due to scattering or medium absorption. In order to illustrate how these typically ignored effects could lead to a wrong estimated temperature value, the emission spectra of SrF_2:Yb,Tm LNThs dispersed in D_2O (to avoid the laser-induced thermal loading caused by the absorption of the 975 nm radiation by H_2O) were measured at different depths in the dispersion volume. In these measurements the

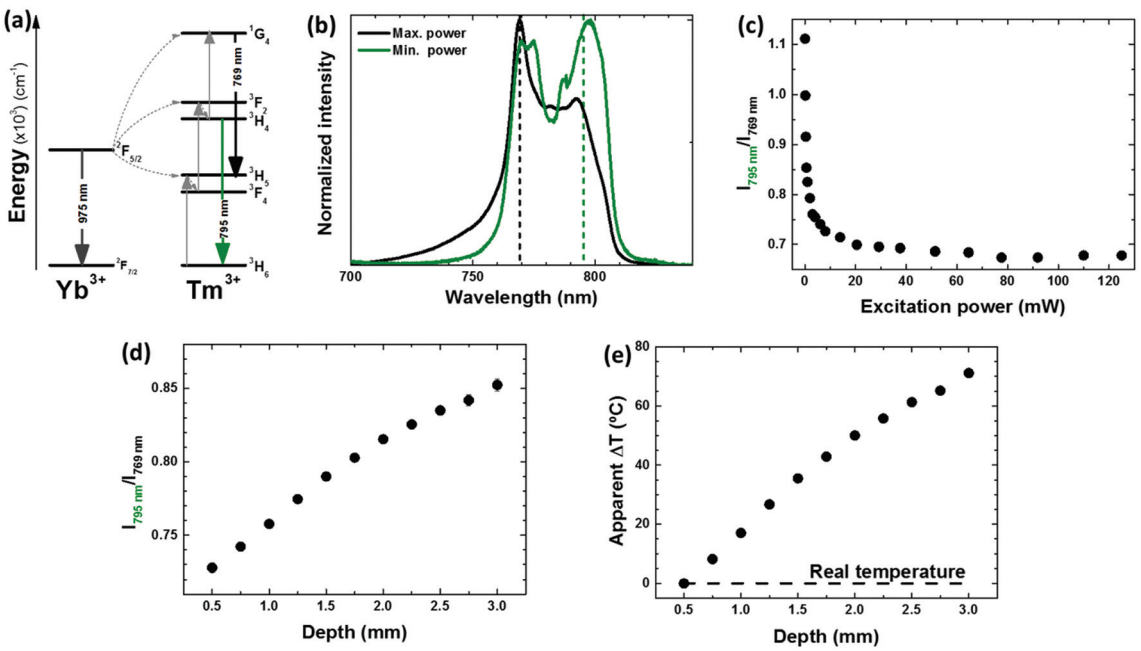

Fig. 2 Excitation power dependence of the emission band shape. (a) Energy level diagram of Tm^{3+} excitation by upconversion (grey) and emissions of interest at around 780 nm (green and black). (b) Emission spectra of SrF_2:Yb,Tm RE-LNThs at around 780 nm under excitation at different powers at 975 nm. Wavelengths of interest for the analysis are pointed out by dashed lines. (c) Ratio of the two emissions in the energy band at around 780 nm for different excitation powers at a fixed depth. (d) Ratio of the two emissions in the energy band at around 780 nm at a fixed applied excitation power for different depths of the excitation/collection focus. (e) TEN, *i.e.* apparent increment of temperature (dots), from the spectral shift with the change of depth due to the excitation power dependence of the emission band shape. The dashed line indicates the real temperature.

975 nm laser power was kept constant leading to a theoretically calculated power density of 8×10^7 mW cm^{-2}. Fig. 2d shows how the ratio between the two emissions constituting the emission band of Tm^{3+} ions increases with depth at a rate of 7.8% mm^{-1}. We attribute this fact to the decrease of the excitation power density with depth due to diverse distance-dependent processes such as the possible aberration of the excitation focal volume, the slight absorption of the excitation light by the dispersion media, and the scattering of photons by the nanoparticles.

These spectral changes produced by artefacts can be falsely attributed to a change in temperature. These effects are so intense that a significant thermal equivalent noise (TEN) appears. TEN is a figure of merit that will be employed along this work to assess the effect of artefacts on the RE-LNThs by considering the apparent variation of temperature due to the change of the parameter responsible for the artefact. The TEN value is given by the variation of the intensity ratio with the parameter producing the artefact divided by the S_R of the LNTh. Fig. 2e shows the TEN or apparent change of temperature that can be obtained from the spectral change with depth due to the excitation power dependence of this emission band of Tm^{3+} ions. Note that although the temperature was the same for all the locations in the cuvette (the same spectrum is expected for different depths) the temperature reading extracted from the analysis of emission spectra gave us an apparent temperature change of 28.7 °C mm^{-1}. Such a high TEN has been obtained for the particular RE-LNThs studied in this work, which are of moderated S_R. The TEN is expected to reduce for larger S_R values. As indicated in Table 2, for the average S_R of the most recent studies on RE-LNThs employing the emission of Tm^{3+} ions,[31–34] their dependence on the excitation power could result in a TEN up to 46.7 °C mW^{-1} at low excitation powers. The lower the applied excitation power, the more sensitive the spectral shape to the variation of the excitation power (see Fig. 2c). Thus, the tendency to reduce the applied excitation power in nanomedicine to minimize the side effects of radiation would lead to an increased dependence of the spectral shape on depth.[53,54]

The actual power density in the focal volume at a certain depth will mainly depend on the deformation of the focal volume with depth due to optical aberrations.[55] This, in turn, would be mainly determined by the NA of the optical system employed for the experiment. The NA is a parameter that accounts for the maximum deviation angle of the collected light with respect to the optical axis. The larger the objective lens NA, the larger the solid angle of the collected luminescence and the smaller the focus diameter. We studied the SrF_2:Yb,Tm spectral shape for objective lenses of different NAs under the same experimental conditions (the applied excitation power density was kept constant at 8×10^7 mW cm^{-2}). Fig. S3a† shows the variation of the intensity ratio with depth for three different NA values. These experimental data reveal that the larger the NA, the more pronounced the induced spectral changes and, therefore, the larger the induced TEN (see Fig. S3b and S3c†). Note that for intracellular thermal sensing experiments the use of high NA is mandatory as high resolution is required. Thus, such measurements would be more affected by the uncontrolled changes in the on-target power density. This effect is systematically ignored in such kinds of measurements although our experimental data indicate that these are not negligible at all.

Note that the effect already described for Yb^{3+} and Tm^{3+} codoped luminescent nanoparticles is also expected to occur for other RE-LNThs. For instance, the Er^{3+} emission at around 550 nm ($^4S_{3/2} \rightarrow {}^4I_{15/2}$, 2 upconversion steps) overlaps with the $^2H_{9/2} \rightarrow {}^4I_{13/2}$ transition (3 upconversion steps). This originates a power dependence of the spectral shape for the emission bands at around 410 and 550 nm.[56,57] In order to prevent RE-LNThs from being affected by this unexpected variation of the emission band shape with the on-target (real) excitation power density, experimental factors enhancing the variation of the excitation power with the depth in the sample volume must be avoided. This includes avoiding the use of high NA objective lenses and the use of excitation at wavelengths overlapping with solvent absorption bands. Special care should also be taken when interpreting spectra from temperature measurements in media with a relevant concentration of scattering agents (such as inhomogeneous tissues). The other source of the artefact could be the heating of the LNThs due to non-radiative de-excitation. If this would happen, there would be an apparent heating with increasing excitation power. In this work, the variation of the spectra with increasing excitation power suggest an apparent cooling of the system (compare Fig. 1g and 2b). Consequently, as the system does not get heated with increasing applied excitation power, we can confirm that this artefact is not taking place. We would like to remark at this point that the possible variation of the signal induced by excitation power density modifications has been systematically ignored in previous studies using RE-LNThs for subcutaneous temperature measurements, to the best of our knowledge.

Table 2 TEN for studies in Table 1 in case they suffer the effect of artefacts studied in this work

RE	Transition	Average S_R	Artefact		TEN	Ref.
Tm^{3+}	$^3H_4 \rightarrow {}^3H_6$	1.05% °C^{-1}	Exc. power	Up to 49% mW^{-1}	Up to 46.7 °C mW^{-1}	31–34
Tm^{3+}	$^3H_4 \rightarrow {}^3H_6$	1.05% °C^{-1}	Exc. power	7.8% mm^{-1}	7.4 °C mm^{-1}	31–34
Nd^{3+}	$^4F_{3/2} \rightarrow {}^4I_{9/2}$	0.30% °C^{-1}	Self-abs.	7.9% mm^{-1}	26 °C mm^{-1}	40–44
Nd^{3+}	$^4F_{3/2} \rightarrow {}^4I_{11/2}$	0.48% °C^{-1}	None	0% mm^{-1}	0 °C mm^{-1}	38
Nd^{3+}	$^4F_{3/2} \rightarrow {}^4I_{13/2}$	0.23% °C^{-1}	Solvent abs.	18% mm^{-1}	78 °C mm^{-1}	37
Yb^{3+}	$^2F_{5/2} \rightarrow {}^2F_{7/2}$	0.37% °C^{-1}	Solvent abs.	17% mm^{-1}	46 °C mm^{-1}	15 and 36
Nd^{3+}	$^4F_{3/2} \rightarrow {}^4I_{13/2}$					

Temperature uncertainties due to RE-LNThs induced by SA

Another artefact that could reduce the reliability of RE-LNThs is the partial absorption of their luminescence by themselves, known as self-absorption (SA) or radiation trapping. As mentioned before, SA occurs when there is a spectral overlap between the emission and the absorption bands of the luminescent material. For rare-earth-doped materials this condition is only fulfilled if the lowest energy level is involved in both absorption and emission processes. This is the case, for instance, of the emission band associated with the $^4F_{3/2} \rightarrow {}^4I_{9/2}$ transition of Nd^{3+} ions (see Fig. 3a) that is, according to Table 1, widely used for luminescence nanothermometry.[39–46] The SrF_2:0.5Nd LNThs studied in this work show a significant overlap of their emission with their excitation spectra, as shown in Fig. 3b. The effect of SA could lead to modifications in the emission band shape not related to temperature variations. This could happen, for instance, when the number of RE-LNThs between the excitation beam focus (where RE-LNThs are emitting) and the detection system is modified. The longer the path travelled by the luminescence through the sample volume, the larger the probability of undergoing SA. This parameter can be modified in colloidal dispersions in a controlled way by changing the excitation light focus depth in the sample volume, as we did to obtain the experimental data shown in Fig. 2. Fig. 3c shows the emission spectra generated by a colloidal dispersion of SrF_2:0.5Nd LNThs as obtained at two different focusing depths in the dispersion, *i.e.* for a short (0.2 mm) and long (3.0 mm) path of the emitted luminescence through the sample volume. In good agreement with the overlap shown in Fig. 3b, the spectrum in Fig. 3c obtained at larger depth differs from the one at a shallow position at the shorter emission wavelengths, where the overlap between emission and absorption is larger. The variation of the emission spectra of the neodymium-doped RE-LNThs is characterized throughout this work by the ratio between the intensity at 769 nm (greatly affected by SA) and that at 803 nm (not affected by SA). The decay of the intensity (I) at a given wavelength with the distance (d) travelled by the luminescence through the colloidal dispersion obeys the Lambert–Beer law, which relates these parameters by means of the absorption (α) of the material at that wavelength.[29] Consequently, the intensity ratio (R) should obey the following behavior:

$$R(d) = \frac{I_{769\ \mathrm{nm}}(d)}{I_{803\ \mathrm{nm}}(d)} = \frac{I_0^{769\ \mathrm{nm}} e^{-\alpha_{769\ \mathrm{nm}} d}}{I_0^{803\ \mathrm{nm}} e^{-\alpha_{803\ \mathrm{nm}}\, d}} = R_0 e^{-(\alpha_{769\ \mathrm{nm}} - \alpha_{803\ \mathrm{nm}})d} = R_0 e^{-\Delta\alpha d} \quad (2)$$

where $R_0 = I_0^{769\mathrm{nm}}/I_0^{803\mathrm{nm}}$ is the intensity ratio obtained when the excitation focus is at the surface of the aqueous dispersion (*i.e.* without suffering from SA) and $\Delta\alpha$ is the difference between the absorption coefficients for our RE-LNThs at 769

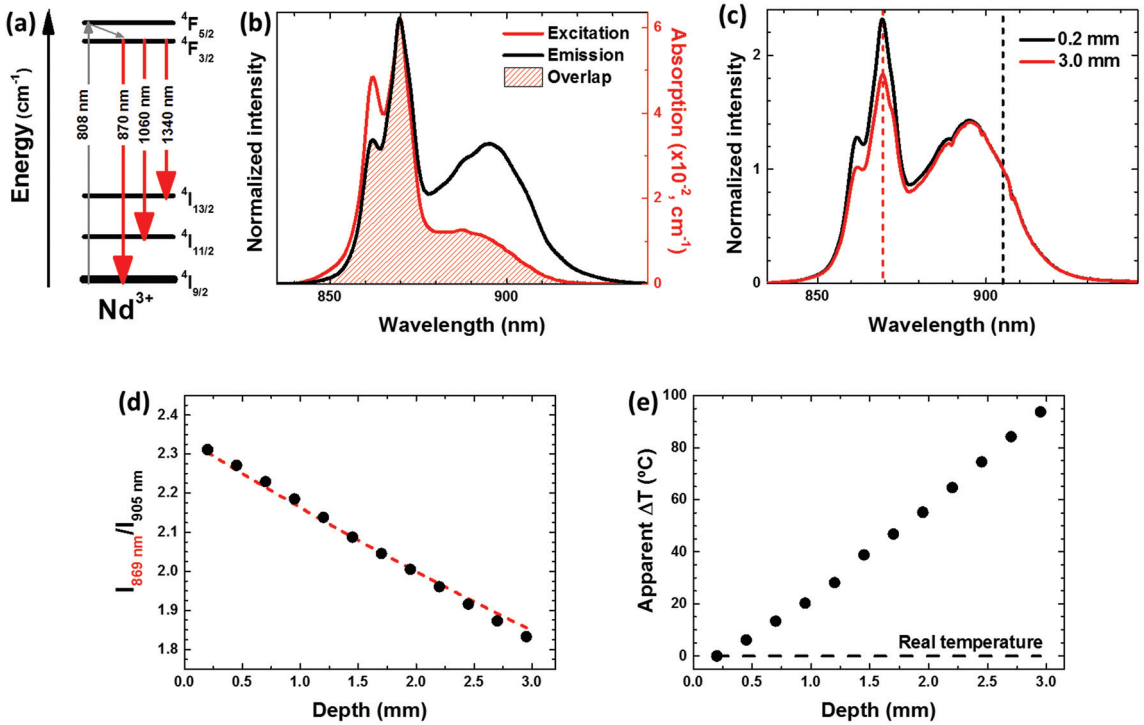

Fig. 3 SA of the luminescence. (a) Energy level diagram of the excitation (grey) and emissions of Nd^{3+} ions in the first biological window (red). (b) Emission spectra of SrF_2:0.5Nd RE-LNThs at around 880 nm under excitation at 808 nm (black) and its overlap (stripped red) with their excitation spectra (red, absorption axis calibrated from the absorption spectra, see Fig. S4†). (c) Emission spectra of SrF_2:0.5Nd RE-LNThs with the excitation/collection focus at different depths in the colloidal dispersion of RE-LNThs. (d) Intensity ratio of this emission at different depths. The dashed line is the fit to the behavior expected by the Lambert–Beer equation (eqn (2)). (e) TEN (dots), *i.e.* apparent increment of temperature, from the spectral shift with the change of depth due to the SA of the luminescence. The dashed line indicates the real temperature.

and 803 nm ($\Delta\alpha = \alpha_{769\ nm} - \alpha_{803\ nm} = 7.9 \times 10^{-3}$ cm^{-1}; see Fig. 3b). As shown in Fig. 3d, the change of the intensity ratio with depth fits well to eqn (2). Thus, the SA in the colloidal dispersion of RE-LNThs obeys the behavior observed before for SA in bulk materials, with an average change of the intensity ratio of 7.9% mm^{-1}. Furthermore, this emission band is originated by a single transition between energy levels and so it is not dependent on the applied excitation power (see Fig. S5†). The experiment in Fig. S5† also proves that these RE-LNThs are not experiencing heating due to non-radiative de-excitations, as the emission spectrum does not change with the excitation power. Therefore, the spectral changes cannot be attributed to the first discussed artefact (caused by uncontrollable changes of the on-target power densities). To test that the observed spectral changes are only due to SA by the RE-LNThs, the change of the emission spectrum with depth for a set of dry RE-LNThs was also measured (Fig. S6†). In this case, due to a much larger concentration of RE-LNThs, the spectral modifications caused by SA were more noticeable, as expected. The magnitude of the spectral modifications caused by SA does not only depend on the concentration of RE-LNThs, but also on the doping level of the individual RE-LNThs. If the doping level is reduced, then the absorption coefficient of each RE-LNTh is also reduced and so the magnitude of SA induced spectral changes. To further test this fact, the SA in an aqueous dispersion of SrF_2:0.22Nd LNThs of the same size and concentration as those of the system studied for previous experiments (SrF_2:0.5Nd) was observed (see Fig. S7†). As expected, a diminished presence of Nd^{3+} ions per LNTh led to a weaker effect of SA. According to these data, for highly reliable temperature measurements, the use of RE-LNThs with low doping levels is advisable. Nevertheless, the use of low doping levels in RE-LNThs usually leads to noisy emission spectra. Thus, the TEN due to SA would be reduced at expenses of an increase in signal noise. As a result of these two effects, the existence of an optimum doping level for each RE-LNTh is expected. This factor has been systematically ignored in the past when designing probes for luminescence nanothermometry applications.

Fig. 3e displays the TEN corresponding to the SrF_2:0.5Nd LNThs due to SA, showing an apparent change of temperature of 34.6 °C mm^{-1}. For the case of the state-of-the-art RE-LNThs employing the emission band of Nd^{3+} ions in the first biological window,[40–44] although their average S_R is larger than that of the system studied in this work, SA would also lead to a significant TEN of 26 °C mm^{-1} (see Table 2). Finally, it should be noted that not only RE-LNThs can undergo SA. Indeed, quantum dots do always present an overlap of their absorption and emission spectra, so they experience an alteration of the emission spectra leading to a red-shift as their luminescence is self-absorbed. Similar effects are also expected to be present during luminescence thermometry measurements based on dyes (such as the well-known rhodamine).

Temperature uncertainties due to medium absorption

Finally, the third effect studied in this work that could lead to false temperature measurements is also related to the absorption of the luminescence, but, in this case, by the medium in which the RE-LNThs are immersed. The scientific community is aware of the side effects of excitation of the luminescence at wavelengths at which water absorbs light. For this reason, great efforts have been made during the last few years to replace Yb^{3+} ions as sensitizers.[17] Moreover, water optical absorption could also produce false readings from RE-LNThs when there is overlap between their emissions and the absorption of water.

As it happened with the SA of the luminescence, the longer the path of the luminescence through the dispersion volume, the more pronounced the optical absorption of the luminescence by the medium. Fig. 4a shows the emission band of SrF_2:0.5Nd LNThs at around 1320 nm ($^4F_{3/2} \rightarrow {}^4I_{13/2}$) and its overlap with the intense absorption band of water at around 1430 nm. Due to this partial overlap, the spectral shape of the emitted light becomes strongly altered in its route from the emitting RE-LNThs towards the detection system (see Fig. 4a). To compare the effect of this artefact on this emission band of Nd^{3+} ions at around 1320 nm with that on the emission band of Yb^{3+} ions at around 980 nm, the emission of SrF_2 with both neodymium and ytterbium ions was analyzed.[58]

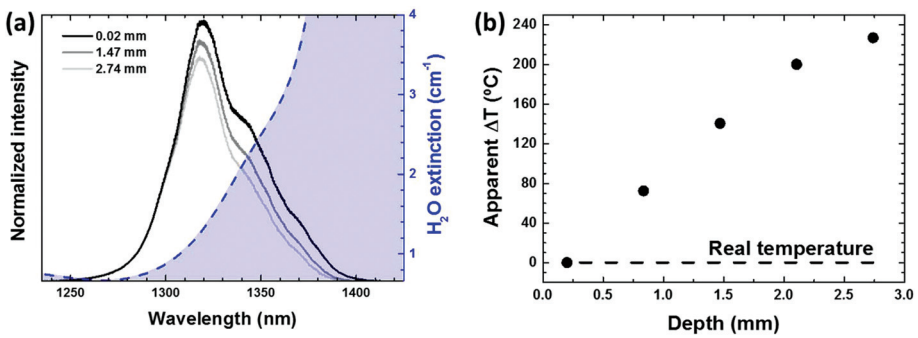

Fig. 4 (a) Emission spectra of SrF_2:0.5Nd RE-LNThs at around 1320 nm under excitation at 808 nm at different excitation/collection focus depths in the colloidal dispersion. The extinction spectra of the solvent (water) are overlapped (dashed blue). (b) TEN (dots), *i.e.* apparent increment of temperature, from the spectral shift with the change of depth due to the absorption of the luminescence by the solvent. The dashed line indicates the real temperature.

Fig. S9† shows the effect of water absorption on the Yb^{3+} emission band at around 980 nm, which is less pronounced than that on the Nd^{3+} emission band at about 1320 nm. Again in the case of Nd^{3+}-doped LNThs, the magnitude of the TEN or apparent increment of temperature induced by the absorption of the 1.3 μm Nd^{3+} luminescence by the solvent (water) is 92 °C mm^{-1}, as shown in Fig. 4b. For the S_R of the state-of-the-art RE-LNThs employing this emission band of Nd^{3+} ions,[37] the TEN (*i.e.* the apparent temperature variation) would be as large as 78 °C mm^{-1} and for the case of nanothermometers employing Nd^{3+} and Yb^{3+} ions,[15,36] it would be 46 °C mm^{-1} (see Table 2). In order to give an estimation of the practical relevance of this effect, we will calculate the possible induced error in temperature estimation that solvent (water) absorption could induce in typical experiments. For instance, for *in vitro* measurements (such as intracellular temperature measurements) cells are placed in water-filled chambers with a typical thickness of 0.2 mm. Therefore, if Nd-doped LNThs are used to measure the temperature at different locations within the chamber, the error induced in temperature estimation due to changes in depth could be as large as 15 °C. Nd-doped LNThs are widely used for *in vivo* applications in which the optical path of luminescence can be as large as several millimeters. In this case, the presence of water in the tissues could lead to an error in temperature estimations of the order of tens of degrees Celsius. Therefore, an adequate selection of the emission bands employed to avoid overlap with a high gradient of the environment absorption, performing *in situ* calibration of the RE-LNThs,[43] and a strict control of the experimental parameters (*e.g.* the depth of the luminescent LNThs in the specimen) are mandatory to avoid induced errors in the emission bands susceptible to be affected by this artefact.

As a summary, Fig. 5 includes the emission bands of SrF_2 luminescent nanoparticles doped with Nd, Yb, Yb–Tm, or Yb–Er, which are the rare-earth ions most commonly employed in nanothermometry for biological applications. The emission bands with a known excitation power dependence are pointed out. Moreover, all emission bands originating from transitions to the fundamental energy levels of these ions (*i.e.* those susceptible to undergo SA) are indicated. Finally, the absorption of human skin (which in the infrared is mainly due to water)[59] is overlapped to these emissions, to show the emission bands susceptible to being altered by the absorption of the environment in biological applications. Thus, only the emission band of Nd^{3+} ions at around 1060 nm, among those lying in the biological windows of transparency of tissues (see these ranges indicated in Fig. 5), is expected to be free of suffering from any of the artefacts studied in this work. As shown in Table 1, this emission band has only been employed for nanothermometry by Kolesnikov *et al.*[38] For all the other cases, the results included in this work clearly state the importance of testing their reliability as potential luminescent nanothermometers. For this purpose (i) the emission at different excitation powers must be checked, (ii) the emission at different depths in the sample volume must be obtained (to rule out SA), and (iii) a calibration in powder and *in situ* must be performed to become aware of the influence of the environment on the LNThs. Furthermore, a higher S_R reduces the TEN of potential artefacts. Additionally, more efficient and tailored LNThs and more sensitive detectors would enhance the penetration depth for *in vivo* applications and reduce noise. Consequently, new strategies in the design of LNThs and detectors are crucial to achieve a substantial increase of their reliability.

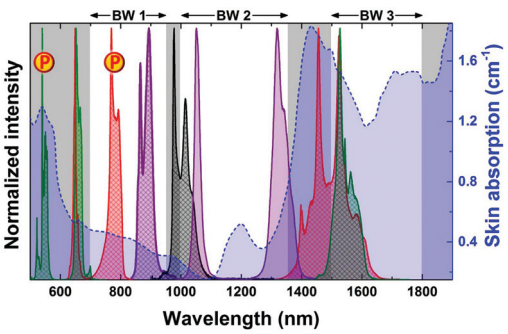

Fig. 5 Normalized emissions of SrF_2:Yb,Er (green), SrF_2:Yb,Tm (red), SrF_2:Nd (purple), and SrF_2:Yb (black) RE-LNThs, where those emission bands susceptible to undergoing SA are pointed out with a grilled filling of the curve. Those emission bands which shape depends on the applied excitation power are indicated by a circular yellow and red warning sign. The absorption of human skin (dashed blue line, data from ref. 55) is overlapped to show the main absorption bands that could alter the emission of the nanoparticles. Grey backgrounds denote the spectral ranges out of the biological windows (BWs) of transparency.

Conclusions

The novel field of luminescence nanothermometry has been consolidated in the last few years, achieving great accuracy and many innovative applications. However, as this work states, there is a challenge to overcome regarding the reliability of luminescent nanothermometers. We have probed the significant influence that diverse artefacts coming from traditionally disregarded effects have on rare-earth-based luminescent nanothermometers. The dependence of the spectral shape on power may induce apparent changes of temperature if the on-target excitation power density is altered by the parameters of the experiment. We have identified the numerical aperture of optics, optical aberrations, and depth variations as factors that unexpectedly induce such artefacts. Moreover, the spectral shape can be modified by partial absorption of the luminescence by the luminescent nanothermometers themselves. This partial self-absorption of the luminescence has been found to produce spectral changes whose magnitude depends on depth and on the concentration of luminescent ions. Furthermore, a spectral modification can be originated by an overlap of the absorption of the environment with the emission of the luminescent nanothermometers. This artefact also induces apparent temperature changes, which are dependent on depth too. All these undesired effects can lead to an error in temperature determination of tens of degrees Celsius.

Almost all the emission bands of rare-earth ions in the biological windows of transparency are expected to be affected by at least one of the artefacts studied in this work. Moreover, quantum dots and dyes are affected to some degree by self-absorption. In conclusion, as these artefacts may affect the majority of the known luminescent nanosensors, it is necessary to assess the reliability of luminescent nanosensors to avoid inducing false spectral changes and, thus, false results. This can be achieved by performing simple tests on the luminescent nanothermometers to identify the sources of artefacts and having more control over the experimental conditions.

Experimental

Synthesis of the LNPs

The LNPs studied in this work were synthesized by a hydrothermal method described in previous studies.[34,58,60]

Transmission electron microscopy

The images were obtained by using a transmission electron microscope (JEM1010, Jeol) and a 4K × 4K digital camera (TemCam-F416, TVIPS).

Spectroscopy setup

Emission spectra were obtained upon excitation by single-mode fiber-coupled laser diodes at 975 nm (LU0975M500, Lumics; for SrF_2:Yb,Tm) or 790 nm (LU0786M250, Lumics, for SrF_2:Nd) (or by using a titanium–sapphire continuous wave laser (3900S, Spectra Physics) for excitation spectra). The diode laser light is collimated into a home-made microscope by a fiber port. Then it is focused using a microscope objective lens (40× NA = 0.6 except for the experiments in Fig. S3†), which also collects the emission of the LNThs. The depth of the focus of the objective lens is controlled by means of a micrometric screw. The emitted luminescence is selected by means of a wavelength selective mirror and a 950 nm short-pass filter or an 830 nm long-pass filter. Finally, the luminescence of the LNThs is analyzed by using a spectrometer (iHR320, Horiba, for Tm^{3+} emission, or Kymera 193i, Andor, for Nd^{3+} emission) and recorded by using a cooled array detector (CCD Synapse, Horiba, or InGaAs iDus, Andor, respectively). The extinction spectrum of the LNThs was recorded with a double-beam absorption spectrometer (Lambda1050, PerkinElmer). Temperature control was achieved by means of a controlled temperature stage (PE120, Linkam) with a resolution of 0.1 °C. The dispersions were maintained for 10 minutes at each particular temperature, so that they were at thermal equilibrium.

Conflicts of interest

There are no conflicts to declare.

Acknowledgements

The work was partially supported by the Ministerio de Economía y Competitividad de España (MAT2016-75362-C3-1-R), by the COST Action CM1403, by the Instituto de Salud Carlos III (PI16/00812), by the Comunidad Autónoma de Madrid (B2017/BMD-3867RENIM-CM), co-financed by the European Structural and Investment Fund, and by the University of Verona (Ricerca di base 2015). L. L.-P. thanks the Universidad Autónoma de Madrid for the "Formación de Personal Investigador (FPI-UAM)" program.

Notes and references

1 D. Jaque and F. Vetrone, *Nanoscale*, 2012, **4**, 4301–4326.
2 B. del Rosal, E. Ximendes, U. Rocha and D. Jaque, *Adv. Opt. Mater.*, 2017, **5**, 1600508.
3 M. Quintanilla and L. M. Liz-Marzán, *Nano Today*, 2018, **19**, 126–145.
4 O. Savchuk, J. Carvajal, C. Brites, L. Carlos, M. Aguilo and F. Diaz, *Nanoscale*, 2018, **10**, 6602–6610.
5 C. D. Brites, M. C. Fuertes, P. C. Angelomé, E. D. Martínez, P. P. Lima, G. J. Soler-Illia and L. D. Carlos, *Nano Lett.*, 2017, **17**, 4746–4752.
6 C. D. Brites, X. Xie, M. L. Debasu, X. Qin, R. Chen, W. Huang, J. Rocha, X. Liu and L. D. Carlos, *Nat. Nanotechnol.*, 2016, **11**, 851–856.
7 C. D. Brites, P. P. Lima, N. J. Silva, A. Millán, V. S. Amaral, F. Palacio and L. D. Carlos, *Nanoscale*, 2013, **5**, 7572–7580.
8 D. Jaque and C. Jacinto, *J. Lumin.*, 2016, **169**, 394–399.
9 E. C. Ximendes, U. Rocha, C. Jacinto, K. U. Kumar, D. Bravo, F. J. López, E. M. Rodríguez, J. García-Solé and D. Jaque, *Nanoscale*, 2016, **8**, 3057–3066.
10 E. C. Ximendes, U. Rocha, B. del Rosal, A. Vaquero, F. Sanz-Rodríguez, L. Monge, F. Ren, F. Vetrone, D. Ma and J. García-Solé, *Adv. Healthcare Mater.*, 2017, **6**, 1601195.
11 H. D. Santos, E. C. Ximendes, M. d. C. Iglesias-de la Cruz, I. Chaves-Coira, B. del Rosal, C. Jacinto, L. Monge, I. Rubia-Rodríguez, D. Ortega and S. Mateos, *Adv. Funct. Mater.*, 2018, **28**, 1803924.
12 F. Vetrone, R. Naccache, A. Zamarrón, A. Juarranz de la Fuente, F. Sanz-Rodríguez, L. Martinez Maestro, E. Martín Rodriguez, D. Jaque, J. García Solé and J. A. Capobianco, *ACS Nano*, 2010, **4**, 3254–3258.
13 A. Sedlmeier and H. H. Gorris, *Chem. Soc. Rev.*, 2015, **44**, 1526–1560.
14 A. Gnach, T. Lipinski, A. Bednarkiewicz, J. Rybka and J. A. Capobianco, *Chem. Soc. Rev.*, 2015, **44**, 1561–1584.
15 E. C. Ximendes, W. Q. Santos, U. Rocha, U. K. Kagola, F. Sanz-Rodríguez, N. Fernández, A. d. S. Gouveia-Neto, D. Bravo, A. M. Domingo and B. del Rosal, *Nano Lett.*, 2016, **16**, 1695–1703.
16 E. C. Ximendes, U. Rocha, T. O. Sales, N. Fernández, F. Sanz-Rodríguez, I. R. Martín, C. Jacinto and D. Jaque, *Adv. Funct. Mater.*, 2017, **27**, 1702249.

17 L. Labrador-Páez, E. C. Ximendes, P. R. Sevilla, D. H. Ortgies, U. Rocha, C. Jacinto, E. M. Rodríguez, P. H. Gonzalez and D. J. Garcia, *Nanoscale*, 2018, **10**, 12935–12956.
18 A. C. Crawford, A. Skuratovsky and M. D. Porter, *Anal. Chem.*, 2016, **88**, 6515–6522.
19 R. D. Boyd, S. K. Pichaimuthu and A. Cuenat, *Colloids Surf., A*, 2011, **387**, 35–42.
20 M. Garcia, E. Fernandez Pinel, J. De la Venta, A. Quesada, V. Bouzas, J. Fernández, J. Romero, M. Martin Gonzalez and J. Costa-Krämer, *J. Appl. Phys.*, 2009, **105**, 013925.
21 S.-Y. Wang, S. Huang and D.-A. Borca-Tasciuc, *IEEE Trans. Magn.*, 2013, **49**, 255–262.
22 J. Grandke, U. Resch-Genger, W. Bremser, L.-A. Garbe and R. J. Schneider, *Anal. Methods*, 2012, **4**, 901–905.
23 F. Auzel, G. Baldacchini, L. Laversenne and G. Boulon, *Opt. Mater.*, 2003, **24**, 103–109.
24 A. Braud, S. Girard, J. Doualan, M. Thuau, R. Moncorgé and A. Tkachuk, *Phys. Rev. B: Condens. Matter*, 2000, **61**, 5280.
25 J. Dong, M. Bass, Y. Mao, P. Deng and F. Gan, *J. Opt. Soc. Am. B*, 2003, **20**, 1975–1979.
26 B. Richards, S. Shen, A. Jha, Y. Tsang and D. Binks, *Opt. Express*, 2007, **15**, 6546–6551.
27 E. Cantelar, G. Torchia, J. Sanz-García, P. Pernas, G. Lifante and F. Cussó, *Phys. Scr.*, 2005, **2005**, 69.
28 R. Xu, Y. Tian, L. Hu and J. Zhang, *Appl. Phys. B: Lasers Opt.*, 2011, **104**, 839–844.
29 C. Pérez-Rodríguez, L. Martín, S. León-Luis, I. Martín, K. K. Kumar and C. Jayasankar, *Sens. Actuators, B*, 2014, **195**, 324–331.
30 P. Rodríguez-Sevilla, H. Rodríguez-Rodríguez, M. Pedroni, A. Speghini, M. Bettinelli, J. G. Solé, D. Jaque and P. Haro-González, *Nano Lett.*, 2015, **15**, 5068–5074.
31 R. Wu, J. Zhou, L. Lei, S. Zhang, Z. Xiao, J. Zhang and S. Xu, *Chem. Phys. Lett.*, 2017, **667**, 206–210.
32 S. Zhou, G. Jiang, X. Li, S. Jiang, X. Wei, Y. Chen, M. Yin and C. Duan, *Opt. Lett.*, 2014, **39**, 6687–6690.
33 A. Pereira, J. Silva, A. Gouveia-Neto and C. Jacinto, *Sens. Actuators, B*, 2017, **238**, 525–531.
34 N.-N. Dong, M. Pedroni, F. Piccinelli, G. Conti, A. Sbarbati, J. E. Ramírez-Hernández, L. M. Maestro, M. C. Iglesias-de la Cruz, F. Sanz-Rodriguez and A. Juarranz, *ACS Nano*, 2011, **5**, 8665–8671.
35 A. Pereira, K. U. Kumar, W. Silva, W. Santos, D. Jaque and C. Jacinto, *Sens. Actuators, B*, 2015, **213**, 65–71.
36 A. Bednarkiewicz, M. Stefanski, R. Tomala, D. Hreniak and W. Strek, *Phys. Chem. Chem. Phys.*, 2015, **17**, 24315–24321.
37 S. Balabhadra, M. Debasu, C. Brites, J. Rocha and L. Carlos, *J. Lumin.*, 2016, **180**, 25–30.
38 I. E. Kolesnikov, A. A. Kalinichev, M. A. Kurochkin, D. V. Mamonova, E. Y. Kolesnikov, A. V. Kurochkin, E. Lähderanta and M. D. Mikhailov, *J. Lumin.*, 2017, **192**, 40–46.
39 U. Rocha, C. Jacinto da Silva, W. Ferreira Silva, I. Guedes, A. Benayas, L. Martinez Maestro, M. Acosta Elias, E. Bovero, F. C. van Veggel and J. A. Garcia Sole, *ACS Nano*, 2013, **7**, 1188–1199.
40 U. Rocha, J. Hu, E. M. Rodríguez, A. S. Vanetsev, M. Rähn, V. Sammelselg, Y. V. Orlovskii, J. G. Solé, D. Jaque and D. H. Ortgies, *Small*, 2016, **12**, 5394–5400.
41 U. Rocha, C. Jacinto, K. U. Kumar, F. J. López, D. Bravo, J. G. Solé and D. Jaque, *J. Lumin.*, 2016, **175**, 149–157.
42 U. Rocha, K. Upendra Kumar, C. Jacinto, J. Ramiro, A. J. Caamano, J. García Solé and D. Jaque, *Appl. Phys. Lett.*, 2014, **104**, 053703.
43 E. Carrasco, B. del Rosal, F. Sanz-Rodríguez, Á. J. de la Fuente, P. H. Gonzalez, U. Rocha, K. U. Kumar, C. Jacinto, J. G. Solé and D. Jaque, *Adv. Funct. Mater.*, 2015, **25**, 615–626.
44 A. Benayas, B. del Rosal, A. Pérez-Delgado, K. Santacruz-Gómez, D. Jaque, G. A. Hirata and F. Vetrone, *Adv. Opt. Mater.*, 2015, **3**, 687–694.
45 D. Wawrzynczyk, A. Bednarkiewicz, M. Nyk, W. Strek and M. Samoc, *Nanoscale*, 2012, **4**, 6959–6961.
46 S. Balabhadra, M. L. Debasu, C. D. Brites, L. A. Nunes, O. L. Malta, J. Rocha, M. Bettinelli and L. D. Carlos, *Nanoscale*, 2015, **7**, 17261–17267.
47 A. Skripka, A. Benayas, R. Marin, P. Canton, E. Hemmer and F. Vetrone, *Nanoscale*, 2017, **9**, 3079–3085.
48 B. del Rosal, U. Rocha, E. Ximendes, E. M. Rodríguez, D. Jaque and J. G. Solé, *Opt. Mater.*, 2017, **63**, 185–196.
49 P. Cortelletti, A. Skripka, C. Facciotti, M. Pedroni, G. Caputo, N. Pinna, M. Quintanilla, A. Benayas, F. Vetrone and A. Speghini, *Nanoscale*, 2018, **10**, 2568–2576.
50 M. Pedroni, P. Cortelletti, I. X. Cantarelli, N. Pinna, P. Canton, M. Quintanilla, F. Vetrone and A. Speghini, *Sens. Actuators, B*, 2017, **250**, 147–155.
51 I. Villa, A. Vedda, I. X. Cantarelli, M. Pedroni, F. Piccinelli, M. Bettinelli, A. Speghini, M. Quintanilla, F. Vetrone and U. Rocha, *Nano Res.*, 2015, **8**, 649–665.
52 H. Rodríguez-Rodríguez, P. Rodriguez Sevilla, E. Martin Rodriguez, D. H. Ortgies, M. Pedroni, A. Speghini, M. Bettinelli, D. Jaque and P. Haro-González, *Small*, 2015, **11**, 1555–1561.
53 K. C. Neuman, E. H. Chadd, G. F. Liou, K. Bergman and S. M. Block, *Biophys. J.*, 1999, **77**, 2856–2863.
54 P. Haro-González, W. T. Ramsay, L. M. Maestro, B. del Rosal, K. Santacruz-Gomez, F. Sanz-Rodríguez, J. Y. Chooi, P. R. Sevilla, M. Bettinelli and D. Choudhury, *Small*, 2013, **9**, 2162–2170.
55 Olympus, https://www.olympus-ims.com/en/microscope/terms/classification/.
56 P. Rodríguez Sevilla, *Optical trapping of upconverting particles: fundamentals and applications*, Doctoral thesis.
57 Y. Cho, S. W. Song, S. Y. Lim, J. H. Kim, C. R. Park and H. M. Kim, *Phys. Chem. Chem. Phys.*, 2017, **19**, 7326–7332.
58 L. Labrador-Páez, M. Pedroni, K. Smits, A. Speghini, F. Jaque, J. García-Solé, D. Jaque and P. Haro-González, *Part. Part. Syst. Charact.*, 2017, **34**, 1700276.
59 A. Bashkatov, E. Genina, V. Kochubey and V. Tuchin, *J. Phys. D: Appl. Phys.*, 2005, **38**, 2543.
60 M. Pedroni, F. Piccinelli, T. Passuello, S. Polizzi, J. Ueda, P. Haro-González, L. Martinez Maestro, D. Jaque, J. García-Solé and M. Bettinelli, *Cryst. Growth Des.*, 2013, **13**, 4906–4913.

